Self-Organized Polyelectrolyte End-Grafted Layers Under Nanoconfinement

Mario Tagliazucchi,[†,‡] Xing Li,[†] Monica Olvera de la Cruz,[‡,§] and Igal Szleifer[*,†,‡]

[†]Department of Biomedical Engineering, Northwestern University, Evanston, Illinois 60208, United States, [‡]Department of Chemistry and Chemistry of Life Processes Institute, Northwestern University, Evanston, Illinois 60208, United States, and [§]Department of Materials Science and Engineering, Northwestern University, Evanston, Illinois 60208, United States

ABSTRACT Layers of end-grafted weak polyelectrolytes in poor solvent self-organize into a rich variety of structures (such as micelles, micelles coexisting with nonaggregated chains, stripes and layers with solvent-filled holes) due to the subtle competition among hydrophobic, electrostatic and steric interactions and the chemical acid—based equilibria of the weak polyelectrolyte. In this work, a molecular theory has been used to systematically study how nanoconfinement modulates the competition among these interactions and, therefore, dictates the morphology of the self-assembled layer. Two different types of confinement were considered and compared: (i) soft lateral confinement due to increasing surface coverage in a planar polyelectrolyte brush and (ii) hard vertical confinement due to the interaction of a planar polyelectrolyte brush with an opposing surface, as typically found in AFM-colloidal-tip and surface-force-apparatus experiments. It is shown that increasing the surface coverage (soft lateral confinement) or compressing the layer with an opposing wall (hard vertical confinement) have a similar qualitative effect on the morphology of the system: both types of nanoconfinement increase the stability of morphologies that extend in one or two dimensions (such as the homogeneous brush, holes and stripes) over nonextended aggregates (such as hemispherical micelles). However, vertical confinement can also lead to pillar-like structures that are not observed in the absence of the opposing wall. Interestingly, the pillar structures, which bridge the grafting and opposing surfaces, may coexist with metastable structures collapsed to the grafting surface only. This coexistence may help to understand the hysteresis commonly observed in surface-force experiments.

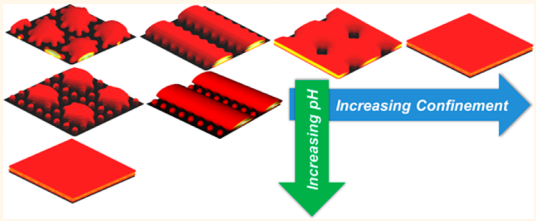

KEYWORDS: molecular interactions · aggregates · poor solvent · polyelectrolyte brush · pH

The behavior of soft materials in confined environments can be very different from bulk solution. This effect has important manifestations in a diverse range of fields from materials science to biology. By confinement, we refer here to the cases where intermolecular distances are constrained, at least in one direction, to length scales comparable or smaller than the size of the molecules or of the relevant intermolecular interactions in free solution. Examples of confined systems include polymer brushes,[1−3] monolayer-protected nanoparticles,[4] as well as molecules that are spatially constrained to a space smaller than the molecular dimensions, such as chain-like molecules within porous solids[5−8] or DNA chains translocating through a nanopore.[9] Confinement introduces a new length scale in the system, for example, the distance between grafting points in a polymer brush or the pore radius in a mesoporous material. These length scales become relevant when they compete with characteristic length scales of the system, such as the size of polymer molecules and the length scale of electrostatic interactions in an electrolyte solution (the Debye length). This competition between length scales dictates the self-organization of confined systems.

Polymers in poor solvent tend to phase separate forming polymer-rich and solvent-rich phases. However, grafted polymers cannot phase separate due to the constraint introduced by the tethering points, and therefore, they microphase separate forming polymer-rich self-organized aggregates and polymer-free regions.[10] Previous experiments,[11,12] computer simulations[13−15] and theory[16−22] have addressed the

* Address correspondence to igalsz@northwestern.edu.

Received for review April 10, 2014 and accepted September 15, 2014.

Published online September 15, 2014
10.1021/nn502008x

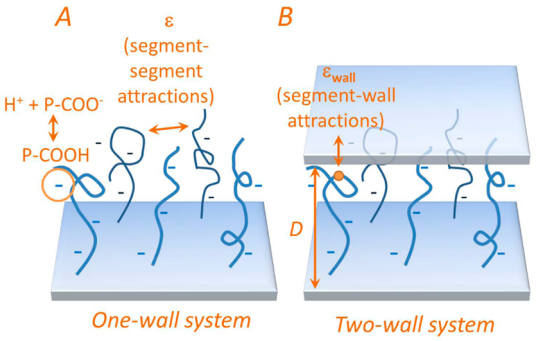

Figure 1. Schematic of the systems under study. In the one-wall system (A), a planar surface is modified by a layer of end-grafted hydrophobic weak polyelectrolytes of length N and surface density σ_P. Each segment in the polyelectrolyte chain bears an acid group; this group can be either in a protonated neutral state (carboxylic acid) or in a deprotonated negatively charged form (carboxylate). The parameter ε is the strength of the effective segment−segment attractions due to the hydrophobicity of the polymer backbone. The system is immersed in an electrolyte aqueous solution of concentration C_{salt} that contains salt ions (anions and cations), water molecules, protons and hydroxyl ions. The two-wall system (B) differs from the one-wall system in the presence of a bare opposing wall located at a distance D from the polyelectrolyte-modified surface. The polyelectrolyte segments experience an effective attraction to the opposing surface; the strength of this attraction is given by the parameter ε_{wall}.

morphology of hydrophobic end-grafted polymers and polyelectrolytes. In our previous work,[16,23] we studied end-grafted weak polyelectrolyte layers in poor solvent and presented the different morphologies that this system can adopt: micelles, stripes, holes and micelles coexisting with isolated chains. The rich morphological behavior observed in this system makes it a very appealing model to study the competition of molecular interactions under nanoconfinement and its consequences on self-assembly.

In the present work, we explore the effects of nanoconfinement on the morphology of weak polyelectrolytes end-grafted to planar surfaces using a molecular theory that allows inhomogeneities in the three spatial dimensions and that explicitly considers the coupling among electrostatic, hydrophobic and entropic interactions, entropic forces and acid−base chemical equilibria. We study and compare two types of confinement: lateral and vertical. The interaction of a polyelectrolyte chain with its neighbors in a polyelectrolyte brush (Figure 1A) leads to soft lateral confinement, which can be augmented by increasing the grafting density in a planar polyelectrolyte brush. On the other hand, the presence of an opposing surface (Figure 1B) leads to hard vertical confinement, where the polyelectrolyte brush is compressed as the distance between the opposing and grafting surfaces decreases. Hard vertical confinement is found in experimental arrangements such as the AFM-colloidal tip,[24−28] the surface-force apparatus[29−32] and optical-traps with polyelectrolyte-modified colloids.[33] We show here that increasing the grafting density of a planar polyelectrolyte brush (lateral confinement) or decreasing the interwall distance (vertical confinement) increases the stability of continuous morphologies, *i.e.*, the hole and stripe morphologies, over the micelles. We developed a simple argument (for lateral confinement and neutral polymers) that explains this observation in terms of the minimization of the polymer/solvent interfacial area. In the case of vertical confinement, we show two new morphologies that do not exist in the single-wall system: pillars and pillars coexisting with nonaggregated chains. These morphologies bridge the opposing and grafting surfaces. We show that in a system where the pillars are the stable morphology (*i.e.*, the global minimum of the free energy), other morphologies may exist as metastable structures (local minima of the free energy). In particular, we argue that the kinetically controlled transition between metastable structures bridging the two walls and structures collapsed on one wall only is relevant to understand the hysteresis typically observed in the force−distance curves determined by AFM and the surface-force apparatus.

RESULTS AND DISCUSSION

Hydrophobic Polyelectrolyte Brushes under Soft Lateral Confinement. In Figure 2A, we show different morphologies predicted with the molecular theory (see Methods section) for the one-wall system (system in Figure 1A). The range of stability of each morphology is shown in Figure 2B as a function of pH, hydrophobicity of the polymer backbone ($\varepsilon_C/\varepsilon$) and surface coverage ($\sigma_P$). Note that the hydrophobicity of the polymer backbone is measured in terms of $\varepsilon_C/\varepsilon$, where ε is the segment−segment attraction strength and ε_C is the critical value of ε required to microphase separate a neutral polymer brush in the limit of vanishing surface coverage.[10,16,34] Thus, large $\varepsilon_C/\varepsilon$ corresponds to good solvent conditions (hydrophilic polymer backbone), while low $\varepsilon_C/\varepsilon$ indicates poor solvent conditions. The equilibrium morphology for large values of $\varepsilon_C/\varepsilon$ is the homogeneous brush, where all chains are equivalent. Increasing the hydrophobicity of the solvent (decreasing $\varepsilon_C/\varepsilon$), induces microphase separation in the layer. The microphase-separated layer can adopt different morphologies: a layer perforated by holes filled with solvent (holes, H), a lamellar-type structure (stripes, S), hemispherical aggregates (micelles, M), as well as morphologies where isolated chains coexists with either micelles (micelles + nonaggregated chains, M+NA) or stripes (stripes + nonaggregated chains, S+NA). In order to analyze systematically the morphology diagrams, let us consider first the limiting case of a neutral polymer, which corresponds to the low-pH regime of our weak polyacid.

Morphology Behavior in the Neutral Polymer Limit. At pH = 3, all segments in the polyacid chain are protonated

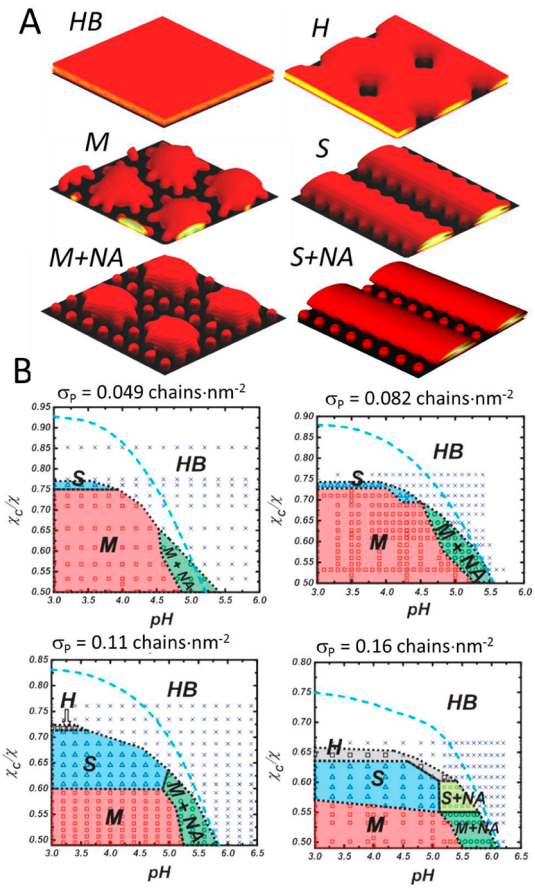

Figure 2. (A) Morphologies predicted by the molecular theory for the one-wall system (Figure 1A), shown as isodensity surfaces. These morphologies are HB (homogeneous brush), H (holes), M (micelles), S (stripes), M+NA (micelles coexisting with nonaggregated chains) and S+NA (stripes coexisting with nonaggregated chains). (B) Morphology diagrams for the one-wall system for $N = 50$, $pK_a = 5$ and $C_{salt} = 0.1$ M for different surface densities of the polyelectrolyte end-grafted chains (σ_P). The morphology diagrams show the equilibrium morphologies in the $\varepsilon_C/\varepsilon$-pH plane, where the parameter $\varepsilon_C/\varepsilon$ determines the hydrophobicity of the polymer backbone: large $\varepsilon_C/\varepsilon$ corresponds to a hydrophilic polymer, whereas small $\varepsilon_C/\varepsilon$ indicates a hydrophobic polymer.

($pK_a = 5$) and, thus, uncharged. Figure 3A shows the morphology diagram of the one-wall system in the $\varepsilon_C/\varepsilon-\sigma_P$ plane for fixed pH = 3. Increasing either $\varepsilon_C/\varepsilon$ or σ_P induces the following morphology transitions: micelles (M) → stripes (S) → holes (H) → homogeneous brush (HB). The predicted effect of σ_P agrees with recent AFM experiments on pNIPAM end-grafted layers, that show the homogeneous brush at high grafting densities and micellar aggregates at low grafting densities.[12]

In order to explain the results in Figure 3A, we consider an approximate two-phase model, where the system is divided into a polymer-free solution phase and a polymer-rich phase with a polymer volume fraction ϕ_P. For a neutral polymer, we obtained an approximate free energy of the system by assuming a two-phase system. This derivation, described in the

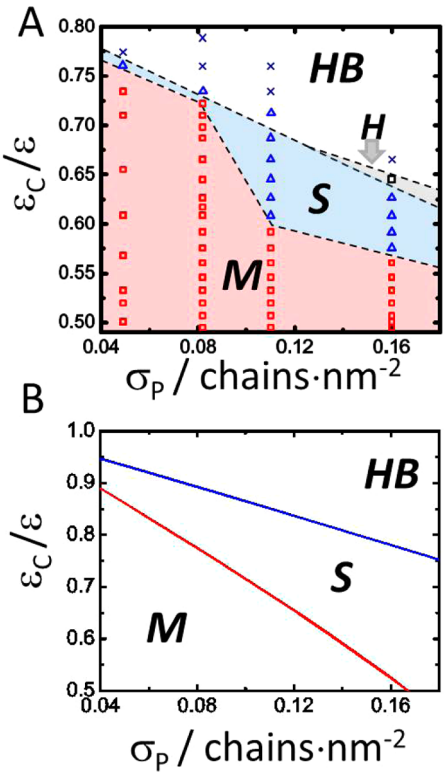

Figure 3. (A) Morphology diagrams for the one-wall system in the $\varepsilon_C/\varepsilon-\sigma_P$ plane for the same conditions as Figure 2B and pH = 3 (neutral polymer), as predicted by the molecular theory calculations. The dashed lines are guides to the eye. (B) Same as A, but predicted by the simple model given by eqs 2, 3 and 4. The morphologies are assigned according the conditions: $1 < \beta F^M/\beta F^{HB}$, $1 < \beta F^S/\beta F^{HB}$ for HB; $\beta F^S/\beta F^{HB} < 1$, $\beta F^S/\beta F^{HB} < \beta F^M/\beta F^{HB}$ for S and $\beta F^M/\beta F^{HB} < 1$, $\beta F^M/\beta F^{HB} < \beta F^S/\beta F^{HB}$ for M (our simple model does not make predictions on the stability of the holes morphology).

Supporting Information (SI), yields the following expression for the free energy per area A of the grating surface:

$$\frac{\beta F}{A} = \frac{N\sigma_P v_P}{\phi_P v_W}[(1-\phi_P)\ln(1-\phi_P)+\phi_P] + \frac{\beta\varepsilon N\sigma_P v_P \phi_P g}{2} - \frac{S}{A}\frac{\beta\varepsilon\phi_P^2 g a}{4} \quad (1)$$

The first term in eq 1 arises from the osmotic pressure of the layer (*i.e.*, the translational entropy of the solvent in the polymer phase). In this term, v_W and v_P are the molecular volumes of the water molecules and the polymer segments, respectively, and N is the number of monomers per polyelectrolyte chain. The second term is the cohesive energy of the polymer phase due to the vdW attractions between segments. In this term, $\beta = 1/k_BT$, and g is a constant (of volume units) which arises from the integration of the vdW segment−segment effective interactions within the volume of the polymer phase. The last term in eq 1 is the interfacial energy between the polymer and solution phases, S is the interfacial area and a is the segment length. This term is effectively the surface tension multiplied by the area written in terms of the

interaction parameters of the molecular theory. The approximate two-phase free energy functional, expressed in eq 1, neglects the conformational entropy of the chains (which includes the stretching entropy of the legs connecting the grafting points to the aggregates[21]). This assumption is based on the fact that the conformational entropy is much smaller than the terms included in eq 1 because our polymers are relatively short ($N = 50$) and the cohesive energy is large due to the hydrophobic nature of the polymer chains.

The most important contributions to the free energy in eq 1 are the osmotic pressure (first term) and the cohesive energy (second term). The competition between these two contributions determines an optimal volume fraction of the polymer in the polymer-rich phase, which depends only on strength of the hydrophobic interactions (*i.e.*, the value of $\varepsilon_C/\varepsilon$). This optimal volume fraction, ϕ_P^{opt}, can be numerically calculated from the following implicit relation:

$$\frac{\varepsilon_C}{\varepsilon} = -\frac{1}{2}\frac{(\phi_P^{opt})^2}{\ln(1-\phi_P^{opt})+\phi_P^{opt}} \quad (2)$$

This result shows that ϕ_P^{opt} is a monotonically decreasing function of $\varepsilon_C/\varepsilon$, (the stronger the segment−segment attractions, the denser the polymer phase). Note that ϕ_P^{opt} is independent of the morphology of the system, and therefore, the shape of the aggregates is determined by minimizing the surface-energy contribution to the free energy (the third term in eq 1) for a fixed polymer volume fraction ϕ_P^{opt}. In the Supporting Information, we show that this minimization yields the following equations that describe the region of thermodynamic stability of the homogeneous brush, the micelles and the stripes morphologies:

$$\frac{\beta F_{surf}^{M}}{\beta F_{surf}^{HB}} = \frac{S^{M}}{S^{HB}} = 2\pi\left(\frac{3}{2\pi}\right)^{2/3}\left(\frac{v_P\sigma_P}{a\phi_P^{opt}}\right)^{2/3} \quad (3)$$

$$\frac{\beta F_{surf}^{S}}{\beta F_{surf}^{HB}} = \frac{S^{S}}{S^{HB}} = \pi\left(\frac{2}{\pi}\right)^{1/2}\left(\frac{v_p\sigma_p}{a\varphi_P^{opt}}\right)^{1/2} \quad (4)$$

In these equations, βF_{surf}^{i} and S^i are the interfacial free energy (given by the third term in eq 1) and the surface area for the morphology i, with i = HB, M or S for the homogeneous brush, micelles and stripes, respectively. We combined eqs 2, 3 and 4 to predict the morphology diagram of the system in the $\varepsilon_C/\varepsilon-\sigma_P$ plane, see Figure 3B. Comparison with the prediction of the full molecular theory calculation (Figure 3A) shows that our simple argument successfully captures the effect of $\varepsilon_C/\varepsilon$ and σ_P on the morphology diagram: (i) increasing $\varepsilon_C/\varepsilon$ or σ_P produces the transitions M → S → HB (note that we did not consider the hole morphology in our simple argument) and (ii) the shape of the boundaries between morphologies predicted by the simple model and the molecular theory calculations are in qualitative agreement. In particular, both calculations agree in the fact that the region of stability of the stripes increases with increasing σ_P.

The success of our two-phase model to capture the self-organization of the weak polyelectrolyte layers (in the uncharged limit) indicates that, given an optimal polymer volume fraction, the equilibrium morphology of the system minimizes the contact area between the polymer and the solution phases. When the optimal polymer volume fraction is small (large $\varepsilon_C/\varepsilon$), the volume of the polymer-phase is large and the surface area is minimized by those morphologies that extend into two dimensions (H and HB). As the optimal density becomes larger (smaller $\varepsilon_C/\varepsilon$), the volume of the polymer phase, V, decreases. In the case of the homogeneous brush the contact area is (in a first approximation) independent of the volume of the polymer phase, *i.e.*, $S^{HB} \sim V^0$. For the stripes, the contact area decreases as V decreases as $S^S \sim V^{1/2}$ and, for the micelles, the contact area decreases as V decreases even faster than for the stripes: $S^M \sim V^{2/3}$. Therefore, as ϕ_P^{opt} increases and V decreases, the morphology of the system will transition from the homogeneous brush to stripes to micelles. The effect of surface coverage, σ_P, on the morphology diagrams is also explained by the arguments above: in order to keep ϕ_P^{opt} constant, the volume of the polymer phase should increase with increasing σ_P. This situation favors the structures with two-dimensional periodicity (holes and homogeneous brush) over the stripes (one-dimensional periodicity) and the stripes over the micelles (noncontinuous aggregates). As we will show below, this argument can also be extended to the case of hard vertical confinement.

Our simple model can be compared to the scaling arguments of Pattanayek *et al.*,[18] who considered the balance between surface tension and chain stretching, but assumed an unity volume fraction for the polymer in the aggregates (*i.e.*, assumed the limit of very small $\varepsilon_C/\varepsilon$). Both our argument and that of Pattanayek *et al.* capture the effect of σ_P on the morphology transitions; however, our argument also captures the effect of the hydrophobicity on the stability of the morphologies, while the scaling argument of Pattanayek *et al.* makes no predictions regarding this point.

Morphology Behavior of Weak Polyelectrolytes. In the previous section, we discussed the morphology behavior of the polyelectrolyte end-grafted layer in the limit of the neutral polymer, which, for the polyacids under study, corresponds to pH ≪ pK_a. Increasing the pH, for low $\varepsilon_C/\varepsilon$, the molecular theory predicts the transitions M → M+NA → HB (see Figure 2B). The M+NA are micellar aggregates coexisting with nonaggregated chains. Within the micellar aggregates, the fraction of carboxylates (deprotonated units) is much smaller than that expected from the bulk pK_a and pH due to charge

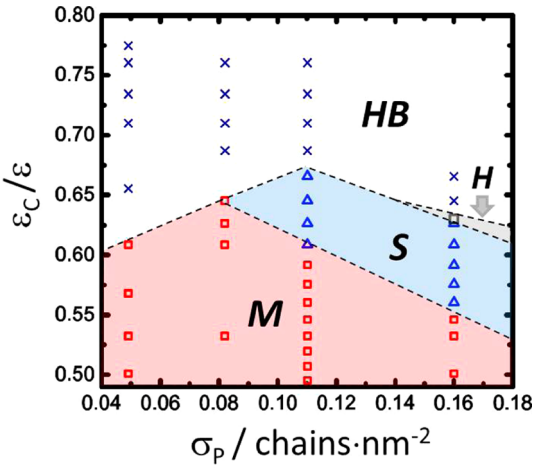

Figure 4. Morphology diagram for the one-wall system in the $\varepsilon_C/\varepsilon-\sigma_P$ plane for pH = 4.5. The dashed lines are guides to the eye.

regulation. In other words, the high segment density within the micelles creates a strong electrostatic repulsion that is alleviated by shifting the acid−base equilibrium of the segments toward the neutral carboxylic acid species. On the other hand, the fraction of charged segments in the nonaggregated chains is substantially larger than that within the micelles (but still lower than that of the bulk solution). The nonaggregated chains adopt extended rod-like conformations in order to minimize segment−segment electrostatic repulsions. As we discussed in ref 16, the coexistence between charged isolated chains and collapsed micelles is a direct consequence of the coupling between the local acid−base equilibrium, the electrostatic and hydrophobic interactions and the molecular organization of the confined chains. Imposing the state of protonation to be uniform, instead of enabling it to vary locally and be a result of the total free-energy minimization, leads to qualitative wrong results. For example, the M+NA morphology is not predicted for neutral polymers or polyelectrolytes with fixed charge density (quenched polyelectrolytes).[16]

Figure 2B shows that increasing the pH above that of the M+NA yields the homogeneous brush, as the electrostatic repulsions overcome the hydrophobic attractions. For the largest surface coverage under study (σ_P = 0.16 chains·nm^{-2}) and intermediate values of $\varepsilon_C/\varepsilon$, we observe the transition S → S+NA → HB upon increasing the bulk pH (Figure 2B). The morphology S+NA, described here for the first time, is the coexistence of stripes and nonaggregated chains. This morphology is similar to the M+NA morphology, described in detail in ref 16. We will return to the study of coexisting aggregated and nonaggregated chains in the analysis of the two-wall system, where pillars coexist with nonaggregated chains.

Figure 4 shows the $\varepsilon_C/\varepsilon$ *vs* σ_P curve for the coexistence of the homogeneous brush and microphase

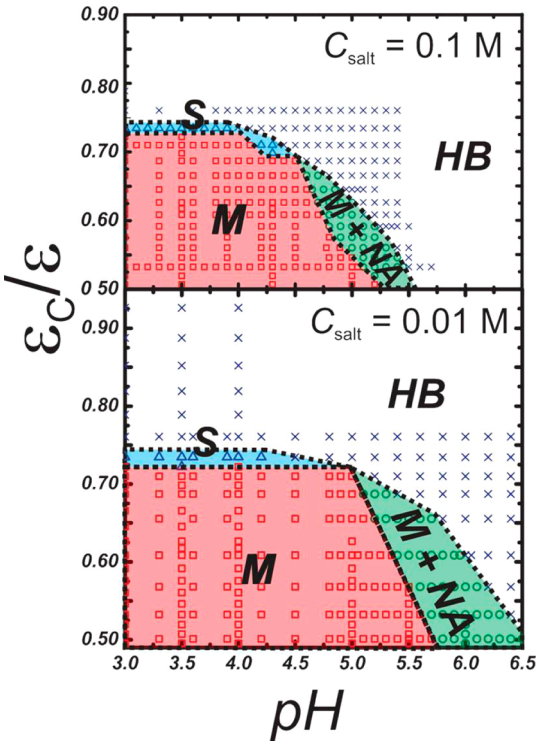

Figure 5. Morphology diagrams for the one-wall system for σ_P = 0.082 chains·nm^{-2} and different bulk salt concentrations (C_{salt}). Other parameters were the same as in Figure 2B.

separated structures for pH = 4.5, note that this curve has a maximum around σ_P = 0.11 chains·nm^{-2}. In the case of pH = 3, we have shown that increasing the surface coverage stabilizes morphologies extended in two and one dimensions. The same effect is observed for charged polyelectrolytes and large surface coverages. However, for low surface coverage, we found the opposite effect: the stability of the homogeneous brush decreases as the surface coverage increases.[34] The reason for this behavior is that increasing σ_P decreases the distance between charged segments and, therefore, increases the electrostatic repulsions. The system reduces these repulsions by shifting the acid−base equilibrium toward the neutral polymer. For example, the average fraction of charged segments (for pH = 4.5 and $\varepsilon_C/\varepsilon$ = 0.53) decreases from 0.084 for σ_P = 0.049 chains·nm^{-2} to 0.059 for σ_P = 0.16 chains·nm^{-2}. Thus, for a given pH, increasing the surface coverage decreases the fraction of charged segments, shifts the system toward the neutral brush and, therefore, stabilizes the microphase-separated morphologies over the homogeneous film.

The concentration of salt plays a key role in modulating the electrostatic interactions in polyelectrolyte layers. Figure 5 shows morphology diagrams for σ_P = 0.086 chains·nm^{-2} and two different salt concentrations (0.1 and 0.01 M). The two diagrams are very similar for pH < 4, where the brush is very weakly charged and the hydrophobic attractions dominate over the weak electrostatic repulsions. On the other

hand, we observe that the M + NA → HB transition shifts to higher pH when decreasing the salt concentration from C_{salt} = 0.1 M to C_{salt} = 0.01 M. Decreasing the salt concentration enhances electrostatic repulsions in the system and, thus, it is expected to stabilize the homogeneous brush with respect to the microphase-separated morphologies; however the opposite effect is observed. The reason for this counterintuitive behavior is that the system mitigates the increase of electrostatic repulsions due to a decrease of the salt concentration by shifting of the acid−base equilibrium of the segments toward the neutral state. For example, the average fraction of charged segments decreases from 0.071 to 0.031 when C_{salt} decreases from 0.1 to 0.01 M (pH = 4.5, σ_P = 0.086 chains·nm^{-2} and $\varepsilon_C/\varepsilon$ = 0.53). The decrease of the fraction of charged segments at low salt concentrations stabilizes the microphase-separated aggregates over the homogeneous brush.[11,34] The effects of C_{salt} and σ_P on the morphology diagrams are, therefore, ruled by the same mechanism.

Hydrophobic Polyelectrolyte Brushes under Vertical Confinement: The Effect of the Opposing Wall. So far, we focused our attention on the effect of lateral confinement on the morphology diagrams of the one-wall system (Figure 1A); we now concentrate on the two-wall case (Figure 1B). Confinement by a hard opposing surface is typically found in AFM-colloidal tip or surface-force apparatus experiments, which have been extensively used to characterize polymer and polyelectrolyte brushes. The opposing surface in these experiments is curved rather than flat. However, the radius of curvature in these systems is in general much larger than any characteristic length scale of the polymer layer, except for small nanoparticle modified tips. Therefore, the grafted layer experiences mainly vertical confinement by a locally flat opposing surface in both AFM-colloidal tip and SFA experimental set ups. The presence of the opposing wall introduces two new variables to the problem: the interwall distance, D, and the strength of the effective interactions between the polymer segments and the opposing wall, ε_{wall}. We consider the possibility of attractive interactions between the polymer segments and the opposing wall based on AFM experiments involving hydrophobic colloidal tips.[27] Note, however, that in all cases the grafting substrate is purely repulsive to the polymer segments.

Figure 6A shows the morphologies of the two-wall system for a hydrophobic polyelectrolyte ($\varepsilon_C/\varepsilon$ = 0.47) at pH = 3 (uncharged segments) and different values of D and ε_{wall}. We observe micelles (M), pillars (P) and holes/stripes (H/S) morphologies. The pillars (P) are bundles of chains that bridge the grafting and the opposing surfaces. This morphology is not observed in one-wall systems. The stripes and holes morphologies are similar to those discussed above for the one-wall

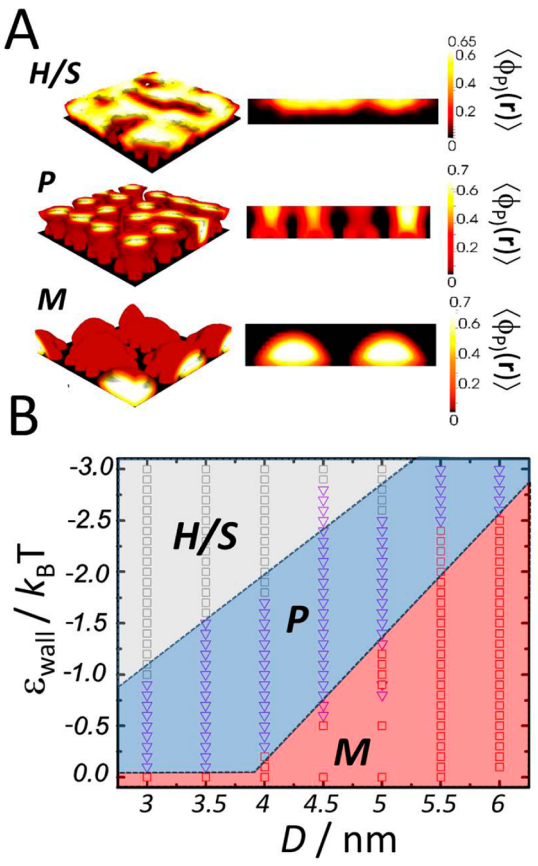

Figure 6. (A) Morphologies observed for the two-wall system (Figure 1B). These morphologies are M (micelles), H/S (stripes or holes) and P (pillars bridging the grafting and opposing surfaces). The figure shows isodensity surfaces of the morphologies (left) and color maps of a plane that cuts the system perpendicular to the grafting and opposing surfaces (right). (B) Morphology diagram of the two-wall system for pH = 3 and pK_a = 5 (neutral polyelectrolyte), σ_P = 0.11 chains·nm^{-2}, N = 50 and $\varepsilon_C/\varepsilon$ = 0.47 (hydrophobic polymer). The diagram shows the equilibrium structures in the ε_{wall}−D plane.

case, but when the opposing wall is attractive (for ε_{wall} < 0), the polymer chains in these morphologies bridge the two surfaces and have a large fraction of their segments in contact with the opposing wall. In many cases it was very difficult to unambiguously classify the result of a calculation as either stripes or holes and thus we decided to group them as the holes/stripes morphology (H/S). Figure 6B shows the morphology diagram of the two-wall system in the D−ε_{wall} plane. For large interwall distances, D, we observe the micelle morphology, which, as expected, is the stable morphology for the one-wall system in the conditions of the diagram (pH = 3 and $\varepsilon_C/\varepsilon$ = 0.47). For large D the entropic cost to stretch the chains to form pillars is too high and thus micelles are obtained. Decreasing D produces the transition from the micelles to the pillars morphology, provided that ε_{wall} < 0. A further decrease in D favors the holes/stripes morphology and eventually (for D < 3 nm, not shown in the diagram) the formation of a homogeneous compressed layer.

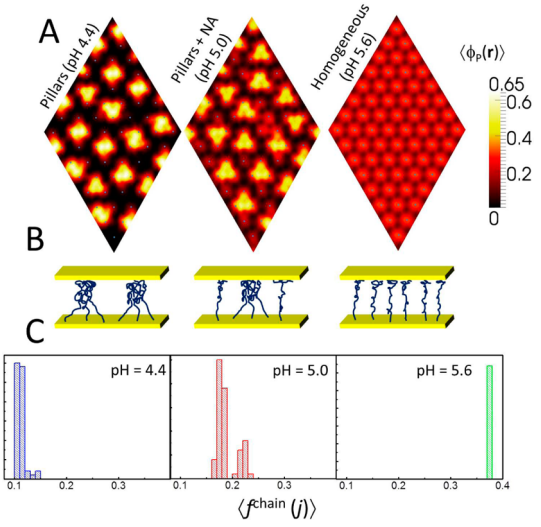

Figure 7. (A) Color maps showing the volume fraction of the polyelectrolyte along the surface of the upper wall for the two-wall system for $\varepsilon_C/\varepsilon = 0.47$, $\varepsilon_{wall} = -3.0\ k_BT$, $D = 7.5$ nm and different pHs. The position of the grafting points is shown with blue points. (B) Schemes of the morphologies for the systems shown in A. (C) Histograms of the average degree of charge per chain ($\langle f^{chain}(j)\rangle$, see eq 4) for the systems in A.

Compressing the polymer aggregates by decreasing D decreases the thickness of the layer. Therefore, in order to maintain the polymer volume fraction in the layer close to its optimal value (ϕ_P^{opt}, see discussion for lateral confinement above) the size of the aggregates in the lateral dimension should increase. As D decreases, this process is responsible for the stabilization of the periodic morphologies, holes and stripe, over the micelles. Previous scaling arguments by Zhulina *et al.* analyzed the compression of a micellar aggregate of end-grafted polymers.[21] This analysis predicted the transition from micelles to homogeneous brush upon decreasing the interwall distance, in agreement with our results. However, their work did not report the hole and stripe morphologies. We attribute this difference to the fact that the scaling analysis requires the consideration of specific morphologies *a priori* and therefore may miss morphology regimes. The molecular theory, on the other hand, makes no *a priori* assumptions about the morphology of the system. The morphology diagram in Figure 6B also shows that increasing the attraction of the segments to the opposing surface (*i.e.*, decreasing ε_{wall}) induces the transitions M → P → H/S, which is explained by the fact that the number of segments in contact with the opposing wall increases in the following order: M < P < H/S.

The diagram in Figure 6B was determined for pH = 3; for pH > 3 we observe the same morphologies as for pH = 3, with one exception: a morphology of pillars coexisting with nonaggregated chains (P+NA), analogous to the M+NA and S+NA morphologies discussed for the one-wall system (Figure 2A). Figure 7A shows color maps for the two-wall system along the plane of the upper surface, for increasing values of the bulk pH and fixed $D = 7.5$ nm. For pH = 4.4, we observe pillars, each one composed of three to five aggregated chains (Figure 7B shows a scheme of this morphology). When the pH increases to 5.0, we observe small spots in the color map of Figure 7A that correspond to single polyelectrolyte chains; these chains are nonaggregated chains; *i.e.*, they do not form part of the pillars. As the pH is increased further to pH = 5.6, there are only nonaggregated chains that form a homogeneous brush bridging both surfaces. In Figure 7C, we show histograms for the average fraction of charged segments of each chain in the system, defined as

$$\langle f^{chain}(j)\rangle = \frac{1}{N}\int \langle n(\mathbf{r},j)\rangle f(\mathbf{r})d\mathbf{r} \qquad (5)$$

where $\langle n(\mathbf{r},j)\rangle$ is the number density of segments of the chain j at position $\mathbf{r}$ and $f(\mathbf{r})$ is the fraction of charged segments at $\mathbf{r}$; for each chain, $0 \le \langle f^{chain}(j)\rangle \le 1$, where $\langle f^{chain}(j)\rangle = 1$ corresponds to a fully charged chain. The average value of $\langle f^{chain}\rangle$ increases, as expected, with increasing bulk pH; however, its distribution (shown in Figure 7C) shows some interesting trends. For pH = 4.4 (pillars) and 5.6 (homogeneous brush), $\langle f^{chain}(j)\rangle$ is monodisperse. On the other hand, for pH = 5.0, $\langle f^{chain}(j)\rangle$ has a bimodal distribution: the chains with large $\langle f^{chain}(j)\rangle$ are nonaggregated and those with small $\langle f^{chain}(j)\rangle$ form part of the pillars. This behavior, equivalent to that described for the M+NA morphology before,[16] is explained by the fact that the polyelectrolyte chains can minimize the free energy of the system either by (i) down-regulating their degree of charge and aggregating into pillars, increasing their cohesive energy or (ii) forming a homogeneous stretched brush with a larger charge than that of the pillars and decreasing their electrostatic repulsions by avoiding aggregation, thus increasing the distance between polymer chains. The interesting prediction of the molecular theory is that for pH = 5.0, some chains in the system will follow the first strategy and others the second; *i.e.*, there is a coexistence between aggregated and nonaggregated chains.

Formation of Metastable Morphologies. Both in the one-wall and two-wall systems, we usually obtain more than one morphology for a given set of system parameters when we solve the molecular theory using different initial guesses for the calculation (*e.g.*, an homogeneous initial guess yields in general the HB morphology). In our morphology diagrams, we report the morphology with the minimum free energy, however, it is insightful to examine the metastable states of the system (structures found in minima of the free energy other that the global minimum). For example, for the two-wall system with $D = 4$ nm and $\varepsilon_{wall} = -1\ k_BT$, the global minima of the free energy is a pillar structure (Figure 8A). Other local minima of the free energy for these values of D and ε_{wall} are the homogeneous film

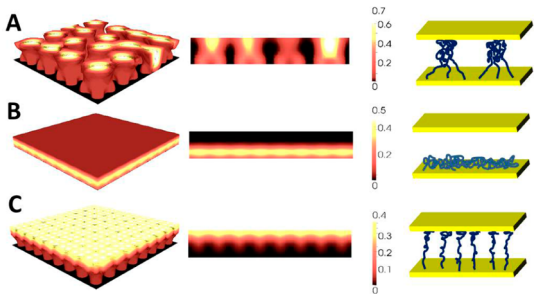

Figure 8. Metastable morphologies for the two-wall system determined for D = 4 nm and $\varepsilon_{wall} = -1.0\ k_BT$ (other conditions were the same as in Figure 6). The pillar morphology (A) is the equilibrium morphology for these conditions (the global minima of the free energy). The morphologies shown in (B) and (C) show a homogeneous brush collapsed to the grafting or the opposing surfaces, respectively. Morphologies (B) and (C) are local minima of the free energy (quasi-equilibrium structures) that have a free energy 0.010 and 0.008 k_BT/chain higher than the free energy of morphology (A), respectively. The morphologies are shown as isodensity plots (right), color maps for cut perpendicular to the grafting and opposing surfaces (center) and schematics (right).

collapsed to the grafting surface (Figure 8B) and the homogeneous film collapsed to the opposing wall (Figure 8C). The free-energy differences between these three morphologies are small, of the order of 0.01 k_BT/chain, and therefore, we speculate that the homogeneous film may coexist with pillars in force−distance experiments. Interestingly, AFM-colloidal-tip experiments of hydrophobic polymer brushes present hysteresis in the force−distance curves:[26−28,35,36] forces recorded during the approach are either repulsive or weakly attractive, while strong attractions arise during retraction of the tip. Therefore, the polymer chains are likely collapsed on the grafting wall during the approaching phase and they bridge the two surfaces during retraction. The metastable morphologies observed in our calculations may be closely related to this experimental behavior since, for a given interwall distance, we observe both morphologies collapsed on the grafting wall (homogeneous brush in Figure 8B) and morphologies bridging the two walls (pillars in Figure 8A and the homogeneous brush collapsed to the opposing surface in Figure 8C). Due to the small differences in free energy, the formation of the metastable structures may strongly depend on the history of the system.

CONCLUSIONS

In this work, we studied the effect of confinement on the morphology behavior of weak polyelectrolyte brushes using a molecular theory. Confining a neutral polymer brush in poor solvent conditions, either by increasing the surface coverage (soft lateral confinement, Figures 2B and 3) or by decreasing the separation between the grafting surfaces (hard vertical confinement, Figure 5B), stabilizes the homogeneous brush over extended microphase-separated morphologies (holes and stripes) and the extended morphologies over isolated aggregates (micelles). We propose that, for neutral polymers and a one-wall system, the morphology of the system is the one that minimizes the surface area for an optimal volume fraction given by the strength of the hydrophobic interactions. In the case of vertical confinement, this argument is still valid, but the hard boundary imposed by the opposing wall and the maximization of the number of segments in contact with this wall (when $\varepsilon_{wall} < 0$) are also important.

In the case of weak polyelectrolytes, the effects of confinement on the hydrophobic interactions, as discussed above, are coupled to the electrostatic interactions and acid−base equilibrium. For instance, decreasing salt concentration or increasing surface coverage stabilizes the formation of aggregates, even though these processes were expected to augment the electrostatic repulsions in the system. This rather counterintuitive result is a consequence of charge down-regulation by displacement of the acid−base equilibrium. Furthermore, the coupling between chemical equilibrium and physical interactions creates a new set of morphologies, where aggregated and nonaggregated chains coexist. While we previously reported one of this morphologies (M+NA),[16] we show here two additional examples (S+NA and P+NA) that demonstrate the general character of this self-organization strategy.

Our theoretical methodology is well-suited for the present study because (i) it explicitly considers the coupling between the physical interactions (electrostatic interactions, short-range hydrophobic attractions and excluded volume repulsions) and chemical equilibria in the system, (ii) it does not assume any morphology *a priori*, but rather the theory finds the morphologies that correspond to local minima of the free energy; the equilibrium morphology is then selected as that of lowest free energy and (iii) its theoretical predictions have been shown to be in good agreement with experimental observables in previous works.[37−41] Despite its many advantages, the theory has a number of limitations. For instance, it does not account for counterion condensation or the effects of heterogeneity of the dielectric function. Counterion condensation is a very important charge-regulation mechanism for highly charged polyelectrolyte chains; however, we expect that this mechanism will be irrelevant in the present case because microphase-separated aggregates exists only for weakly charged polyelectrolytes. The extension of the molecular theory to account for ion condensation has been presented and the predictions are in good agreement with Monte Carlo simulations;[42] however, the inclusion of counterion condensation requires the input of the free energy of condensation, which is usually unknown. Moreover, nonlinear effects such as ion-condensation are most

important in the presence of multivalent (*i.e.*, divalent) ions, in which case, ion-condensation can be included by extending the two-state model to account for the fraction of ions condensed self-consistently, which is an approach that has successfully described the collapse of polyelectrolytes in multivalent salts if ion-correlations are included.[43,44] We also expect, based on previous studies, a negligible effect of the heterogeneity of the dielectric function and the Born energy on the morphology of the polyelectrolyte layer.[41,45] Again, these effects are important when considering strongly charged polyelectrolytes in low salt concentration regimes.[46]

Our findings provide a base for future experiments and modeling by discussing the general mechanisms that control the morphology of weak polyelectrolyte films under nanoconfinement. For instance, the metastable morphologies observed in Figure 7 may help to explain the hysteresis observed in various AFM pulling experiments.[26−28,35,36] Also, our work may facilitate experimental studies of phase behavior: only the homogeneous brush and micelle morphologies, which occupy the largest regions in the morphology diagrams, have been experimentally characterized for homopolymer brushes.[11,12] Grafted films of hydrophobic weak polyelectrolytes exhibit a very rich spectrum of self-organizing regimes due to the competition between different chemical and physical process. Experimental realization of these morphological regimes may open the door to new methodologies for surface self-patterning, which, so far, is mainly restricted to the realm of block copolymers.

METHODS

We model hydrophobic weak polyacids end-grafted to a planar substrate either in the absence (Figure 1A) or presence (Figure 1B) of an opposing wall. The system is immersed in an aqueous solution of salt ions, protons and hydroxyl ions. We study this system with a previously developed molecular theory,[16,41,47] which considers the size, charge, charge distribution, shape and conformations of all molecular species in the system, their electrostatic and nonelectrostatic inter- and intramolecular interactions and the presence of coupled chemical equilibria. The predictions of the theory have been shown to quantitatively describe the structural[48] and functional[37−39] properties of grafted polyelectrolyte layers.

We formulate the molecular theory by writing down an approximate free energy for the system as a functional of the probability of the chain conformations, the distribution of all the molecular species, the position-dependent protonation state and the electrostatic potential. This free energy explicitly accounts for the coupling between the molecular organization, the physical interactions and the chemical state of the system. The distributions are obtained by finding the extremum of the free energy functional with respect to the position-dependent densities of all mobile species, the probability distributions of the polyelectrolyte chains, the position-dependent electrostatic potential and the fraction of protonated/deprotonated segments. More explicitly, the free energy functional for the systems in Figure 1 is

$$\begin{aligned}\beta F =& \int \rho_W(\mathbf{r})(\ln(\rho_W(\mathbf{r})v_W) - 1)d\mathbf{r} + \int \rho_A(\mathbf{r})(\ln(\rho_A(\mathbf{r})v_W) - 1)d\mathbf{r} \\ &+ \int \rho_C(\mathbf{r})(\ln(\rho_C(\mathbf{r})v_W) - 1)d\mathbf{r} \\ &+ \int \rho_{H^+}(\mathbf{r})(\ln(\rho_{H^+}(\mathbf{r})v_W) - 1 + \mu^0_{H^+})d\mathbf{r} \\ &+ \int \rho_{OH^-}(\mathbf{r})(\ln(\rho_{OH^-}(\mathbf{r})v_W) - 1 + \mu^0_{OH^-})d\mathbf{r} \\ &+ \sum_j^{N_p}\sum_\alpha P_P(j,\alpha)\ln(P_P(j,\alpha)) \\ &+ \iint \frac{\beta\varepsilon}{2} g(|\mathbf{r}-\mathbf{r}'|)\langle\phi_P(\mathbf{r})\rangle\langle\phi_P(\mathbf{r}')\rangle d\mathbf{r}d\mathbf{r}' \\ &+ \int \left[\langle\rho_Q(\mathbf{r})\rangle\beta\psi(\mathbf{r}) - \frac{1}{2}\varepsilon_r\beta(\nabla\psi(\mathbf{r}))^2\right]d\mathbf{r} \\ &+ \int \frac{1}{v_P}\langle\phi_P(\mathbf{r})\rangle([f(\mathbf{r})(\ln(f(\mathbf{r})) + \beta\mu^0_{Ac^-}] + (1-f(\mathbf{r}))[\ln(1-f(\mathbf{r})) + \beta\mu^0_{HAc}])d\mathbf{r} \\ &+ \int \frac{1}{v_P}\langle\phi_P(\mathbf{r})\rangle\beta\varepsilon_{wall}g_{wall}(\mathbf{r})d\mathbf{r} \end{aligned} \quad (6)$$

where $\beta = 1/k_BT$ is the inverse temperature. The first five integrals in eq 6 are the translational entropy of water, anions, cations, protons, and hydroxyl ions, respectively. The position-dependent number density of these species is ρ_i, their molecular volume is v_i and their standard chemical potential is μ_i^0, where i is A, C, H^+, OH^- or W for the anions, cations, protons, hydroxyl ions and water molecules, respectively. The sixth term represents the conformational entropy of the polymer chains; in this term $P_P(j,\alpha)$ is the probability of having the polyelectrolyte chain grafted at j in the conformation α. The summation over α is over all possible conformations, while the summation over j is over all the grafting points in the system. The seventh term is the effective van der Waals (vdW) attractive energy of the polymers, where $\langle\phi_P(\mathbf{r})\rangle$ is the volume fraction occupied by polyelectrolyte segments at $\mathbf{r}$, ε is the strength of the effective segment−segment vdW attractions (the strength of the attractions increases as ε becomes more negative), $g(|\mathbf{r}-\mathbf{r}'|)$ is the functional form of the segment−segment attractions (see SI) and v_P is the molecular volume of a polymer segment. The eighth term in eq 6 is the electrostatic contribution to the free energy. In this term, $\psi(\mathbf{r})$ is the electrostatic potential at $\mathbf{r}$, ε_r is the relative (static) dielectric constant of the medium and $\langle\rho_Q(\mathbf{r})\rangle$ is the average charge density at $\mathbf{r}$, which has contributions from the charge densities of the cations, anions, protons, hydroxyl ions and charged polyelectrolyte segments at $\mathbf{r}$. The ninth term models the free energy of the acid−base chemical equilibria of the polyelectrolyte segments, $f(\mathbf{r})$ is the fraction of charged (unprotonated) carboxylates at $\mathbf{r}$. The last term in eq 6 is the interaction between the polyelectrolyte segments and the opposing wall, where ε_{wall} is the strength of the attraction (the more negative ε_{wall}, the stronger the attraction of the segments and the confining surface) and $g_{wall}(\mathbf{r})$ is the functional form of segment-wall interaction. We model $g_{wall}(\mathbf{r})$ using a square well potential: $g_{wall}(\mathbf{r}) = 1$ if $|\mathbf{r} - \mathbf{r}_{surf}| < \delta$ and $g_{wall}(\mathbf{r}) = 0$ otherwise, where $\mathbf{r}_{surf}$ is the point on the upper surface closest to $\mathbf{r}$ and $\delta = 0.5$ nm.

Minimization of the free energy functional is subject to packing constraints that model the excluded volume intermolecular repulsions in the system:

$$\rho_A(\mathbf{r})v_A + \rho_C(\mathbf{r})v_C + \rho_{H^+}(\mathbf{r})v_{H^+} + \rho_{OH^-}(\mathbf{r})v_{OH^-} + \rho_W(\mathbf{r})v_W + \langle\phi_P(\mathbf{r})\rangle = 1 \quad (7)$$

as well as a global electroneutrality constraint:

$$\int \langle\rho_Q(\mathbf{r})\rangle d\mathbf{r} = 0 \quad (8)$$

The packing and global electroneutrality constraints are enforced by introducing the Lagrange multipliers $\pi(\mathbf{r})$ and λ, respectively. We include these constraints and the fact that the polymer layer is in equilibrium with a solution of a given pH and ionic strength; *i.e.*, the chemical potentials of anions and

cations are constant everywhere, in the following semigrand potential:

$$\beta W = \beta F + \int \beta\pi(\mathbf{r})[\sum_i \rho_i(\mathbf{r})v_i + \langle\phi_P(\mathbf{r})\rangle - 1]d\mathbf{r} + \lambda \int \langle\rho_Q(\mathbf{r})\rangle d\mathbf{r} - \beta\mu_C \int \rho_C(\mathbf{r})d\mathbf{r} - \beta\mu_A \int \rho_A(\mathbf{r})d\mathbf{r} \quad (9)$$

Finding the extremum of the functional leads to explicit expressions for the distributions (see SI for details); for example, the probability distribution function of chain conformations is given by

$$P_P(j,\alpha) = \frac{1}{\xi(j)}\exp\left[- \int n_P(\mathbf{r},\alpha,j)(\ln(f(\mathbf{r})) + q_A - \beta\psi(\mathbf{r}) + \beta\mu_A^0 - + v_P\beta\pi(\mathbf{r}) + \beta\varepsilon_{wall}g_{wall}(\mathbf{r}) + \int \beta\varepsilon g(|\mathbf{r} - \mathbf{r}'|)\langle\phi(\mathbf{r}')\rangle d\mathbf{r}')d\mathbf{r}\right] \quad (10)$$

where $n_P(\mathbf{r}, \alpha, j)d\mathbf{r}$ is the number of segments that a chain grafted at j and in conformation α has in the volume element between $\mathbf{r}$ and $\mathbf{r} + d\mathbf{r}$. eq 10 clearly shows in the Boltzmann factor the coupling that exists between the intermolecular interactions, the chemical state and molecular organization.

The determination of $\psi(\mathbf{r})$, $\rho_i(\mathbf{r})$, $f(\mathbf{r})$ and $P_P(j, \alpha)$ for each set of conditions, *e.g.*, solution ionic strength, pH, polymer surface coverage and chain length, *etc*., requires the numerical solution of a set of integrodifferential equations, which include the Poisson equation and the packing constraints. The inputs of the theory are the properties of the polyelectrolyte (chain length, grafting surface density, the hydrophobicity and pK_a of the segments and the molecular volume of the segments), the properties of the solution (salt concentration and pH) and a large set of random self-avoiding polymer conformations which are not allowed to cross the opposing and grafting walls. Upon solving the theory, we obtain information on the structure (density of each molecular species, position-dependent fraction of protonated segments, electrostatic potential) and the thermodynamics (free energy) of the system. We refer the reader to the SI and our previous work[16] for a thorough description on the formulation of the theory and its solving process.

Conflict of Interest: The authors declare no competing financial interest.

Acknowledgment. This material is based upon work supported as part of the NERC (Non-Equilibrium Research Center), an Energy Frontier Research Center funded by the U.S. Department of Energy, Office of Science, Office of Basic Energy Sciences under Award Number DE-SC0000989. This research was supported in part through the computational resources and staff contributions provided by the Quest high performance computing facility at Northwestern University, which is jointly supported by the Office of the Provost, the Office for Research, and Northwestern University Information Technology.

Supporting Information Available: Minimization of the free energy functional, numerical implementation and molecular model; derivation of the two-phase free energy functional for a neutral polymer; analysis of the competition between osmotic pressure and cohesive energy and determination of the interfacial free energy for the homogeneous brush, micelles and stripes. This material is available free of charge *via* the Internet at http://pubs.acs.org.

REFERENCES AND NOTES

1. Advincula, R. C.; Brittain, W. J.; Caster, K. C.; Rühe, J. *Polymer Brushes: Synthesis, Characterization, Applications*; Wiley-VCH: Weinheim, 2005.
2. Azzaroni, O. Polymer Brushes Here, There, and Everywhere: Recent Advances in Their Practical Applications and Emerging Opportunities in Multiple Research Fields. *J. Polym. Sci. Part A: Polym. Chem. 2* **2012**, *50*, 3225–3258.
3. Jonas, A. M.; Hu, Z. J.; Glinel, K.; Huck, W. T. S. Effect of Nanoconfinement on the Collapse Transition of Responsive Polymer Brushes. *Nano Lett.* **2008**, *8*, 3819–3824.
4. Templeton, A. C.; Wuelfing, W. P.; Murray, R. W. Monolayer-Protected Cluster Molecules. *Acc. Chem. Res.* **1999**, *33*, 27–36.
5. Soler-Illia, G. J. A. A.; Azzaroni, O. Multifunctional Hybrids by Combining Ordered Mesoporous Materials and Macromolecular Building Blocks. *Chem. Soc. Rev.* **2011**, *40*, 1107–1150.
6. Wu, Y. Y.; Cheng, G. S.; Katsov, K.; Sides, S. W.; Wang, J. F.; Tang, J.; Fredrickson, G. H.; Moskovits, M.; Stucky, G. D. Composite Mesostructures by Nano-Confinement. *Nat. Mater.* **2004**, *3*, 816–822.
7. Peleg, O.; Tagliazucchi, M.; Kroeger, M.; Rabin, Y.; Szleifer, I. Morphology Control of Hairy Nanopores. *ACS Nano* **2011**, *5*, 4737–4747.
8. Dimitrov, D. I.; Milchev, A.; Binder, K. Polymer Brushes in Cylindrical Pores: Simulation *Versus* Scaling Theory. *J. Chem. Phys.* **2006**, *125*, 034905.
9. Dekker, C. Solid-State Nanopores. *Nat. Nanotechnol.* **2007**, *2*, 209–215.
10. Carignano, M. A.; Szleifer, I. Pressure Isotherms, Phase-Transition, Instability, and Structure of Tethered Polymers in Good, Theta, and Poor Solvents. *J. Chem. Phys.* **1994**, *100*, 3210–3223.
11. Koutsos, V.; vanderVegte, E. W.; Pelletier, E.; Stamouli, A.; Hadziioannou, G. Structure of Chemically End-Grafted Polymer Chains Studied by Scanning Force Microscopy in Bad-Solvent Conditions. *Macromolecules* **1997**, *30*, 4719–4726.
12. Choi, B. C.; Choi, S.; Leckband, D. E. Poly(N-Isopropyl Acrylamide) Brush Topography: Dependence on Grafting Conditions and Temperature. *Langmuir* **2013**, *29*, 5841–5850.
13. Carrillo, J.-M. Y.; Dobrynin, A. V. Morphologies of Planar Polyelectrolyte Brushes in a Poor Solvent: Molecular Dynamics Simulations and Scaling Analysis. *Langmuir* **2009**, *25*, 13158–13168.
14. Sandberg, D. J.; Carrillo, J.-M. Y.; Dobrynin, A. V. Molecular Dynamics Simulations of Polyelectrolyte Brushes: From Single Chains to Bundles of Chains. *Langmuir* **2007**, *23*, 12716–12728.
15. Grest, G. S.; Murat, M. Structure of Grafted Polymeric Brushes in Solvents of Varying Quality—A Molecular-Dynamics Study. *Macromolecules* **1993**, *26*, 3108–3117.
16. Tagliazucchi, M.; de la Cruz, M. O.; Szleifer, I. Self-Organization of Grafted Polyelectrolyte Layers *Via* the Coupling of Chemical Equilibrium and Physical Interactions. *Proc. Natl. Acad. Sci. U. S. A.* **2010**, *107*, 5300–5305.
17. Pattanayek, S. K.; Pereira, G. G. Shape of Micelles Formed from Strongly Adsorbed Grafted Polymers in Poor Solvents. *Macromol. Theory Simul.* **2005**, *14*, 347–357.
18. Pattanayek, S. K.; Pham, T. T.; Pereira, G. G. Morphological Structures Formed by Grafted Polymers in Poor Solvents. *J. Chem. Phys.* **2005**, *122*, 214908.
19. Sevick, E. M.; Williams, D. R. M. Polymers Grafted onto Strongly Adsorbing Surfaces in Poor Solvents: Stretching, Fission, Phase Separation, and Globular Micelles in 2d. *Phys. Rev. Lett.* **1999**, *82*, 2701–2704.
20. Williams, D. R. M. Grafted Polymers in Bad Solvents - Octopus Surface Micelles. *J. Phys. II* **1993**, *3*, 1313–1318.
21. Zhulina, E.; Singh, C.; Balazs, A. C. Behavior of Tethered Polyelectrolytes in Poor Solvents. *J. Chem. Phys.* **1998**, *108*, 1175–1183.
22. Zhulina, E. B.; Birshtein, T. M.; Priamitsyn, V. A.; Klushin, L. I. Inhomogeneous Structure of Collapsed Polymer Brushes under Deformation. *Macromolecules* **1995**, *28*, 8612–8620.
23. Tagliazucchi, M.; Calvo, E. J.; Szleifer, I. Molecular Modeling of Responsive Polymer Films. *AIChE J.* **2010**, *56*, 1952–1959.
24. Drechsler, A.; Synytska, A.; Uhlmann, P.; Stamm, M.; Kremer, F. Tuning the Adhesion of Silica Microparticles to a Poly-(2-Vinyl Pyridine) Brush: An Afm Force Measurement Study. *Langmuir* **2012**, *28*, 15555–15565.
25. Sui, X. F.; Chen, Q.; Hempenius, M. A.; Vancso, G. J. Probing the Collapse Dynamics of Poly(N-Isopropylacrylamide) Brushes by Afm: Effects of Co-Nonsolvency and Grafting Densities. *Small* **2011**, *7*, 1440–1447.

26. Svetushkina, E.; Puretskiy, N.; Ionov, L.; Stamm, M.; Synytska, A. A Comparative Study on Switchable Adhesion between Thermoresponsive Polymer Brushes on Flat and Rough Surfaces. *Soft Matter* **2011**, *7*, 5691–5696.
27. Ishida, N.; Kobayashi, M. Interaction Forces Measured between Poly(N-Isopropylacrylamide) Grafted Surface and Hydrophobic Particle. *J. Colloid Interface Sci.* **2006**, *297*, 513–519.
28. Drechsler, A.; Synytska, A.; Uhlmann, P.; Elmahdy, M. M.; Stamm, M.; Kremer, F. Interaction Forces between Micro-sized Silica Particles and Weak Polyelectrolyte Brushes at Varying pH and Salt Concentration. *Langmuir* **2010**, *26*, 6400–6410.
29. Maeda, N.; Chen, N. H.; Tirrell, M.; Israelachvili, J. N. Adhesion and Friction Mechanisms of Polymer-on-Polymer Surfaces. *Science* **2002**, *297*, 379–382.
30. Zappone, B.; Ruths, M.; Greene, G. W.; Jay, G. D.; Israelachvili, J. N. Adsorption, Lubrication, and Wear of Lubricin on Model Surfaces: Polymer Brush-Like Behavior of a Glycoprotein. *Biophys. J.* **2007**, *92*, 1693–1708.
31. Dunlop, I. E.; Briscoe, W. H.; Titmuss, S.; Jacobs, R. M. J.; Osborne, V. L.; Edmondson, S.; Huck, W. T. S.; Klein, J. Direct Measurement of Normal and Shear Forces between Surface-Grown Polyelectrolyte Layers. *J. Phys. Chem. B* **2009**, *113*, 3947–3956.
32. Balastre, M.; Li, F.; Schorr, P.; Yang, J. C.; Mays, J. W.; Tirrell, M. V. A Study of Polyelectrolyte Brushes Formed from Adsorption of Amphiphilic Diblock Copolymers Using the Surface Forces Apparatus. *Macromolecules* **2002**, *35*, 9480–9486.
33. Elmahdy, M. M.; Synytska, A.; Drechsler, A.; Gutsche, C.; Uhlmann, P.; Stamm, M.; Kremer, F. Forces of Interaction between Poly(2-Vinylpyridine) Brushes as Measured by Optical Tweezers. *Macromolecules* **2009**, *42*, 9096–9102.
34. Gong, P.; Genzer, J.; Szleifer, I. Phase Behavior and Charge Regulation of Weak Polyelectrolyte Grafted Layers. *Phys. Rev. Lett.* **2007**, *98*, 018302.
35. Gotsmann, B.; Fuchs, H. The Measurement of Hysteretic Forces by Dynamic Afm. *Appl. Phys. A: Mater. Sci. Process.* **2001**, *72*, S55–S58.
36. Kober, M.; Sahagun, E.; Fuss, M.; Briones, F.; Luna, M.; Saenz, J. J. Adhesion Hysteresis in Dynamic Atomic Force Microscopy. *Phys. Status Solidi RRL* **2008**, *2*, 138–140.
37. Tagliazucchi, M.; Azzaroni, O.; Szleifer, I. Responsive Polymers End-Tethered in Solid-State Nanochannels: When Nanoconfinement Really Matters. *J. Am. Chem. Soc.* **2010**, *132*, 12404–12411.
38. Tagliazucchi, M.; Calvo, E. J.; Szleifer, I. Molecular Theory of Chemically Modified Electrodes by Redox Polyelectrolytes under Equilibrium Conditions: Comparison with Experiment. *J. Phys. Chem. C* **2008**, *112*, 458–471.
39. Tagliazucchi, M.; Calvo, E. J.; Szleifer, I. Redox and Acid-Base Coupling in Ultrathin Polyelectrolyte Films. *Langmuir* **2008**, *24*, 2869–2877.
40. Wang, D. W.; Nap, R. J.; Lagzi, I.; Kowalczyk, B.; Han, S. B.; Grzybowski, B. A.; Szleifer, I. How and Why Nanoparticle's Curvature Regulates the Apparent pK(a) of the Coating Ligands. *J. Am. Chem. Soc.* **2011**, *133*, 2192–2197.
41. Nap, R.; Gong, P.; Szleifer, I. Weak Polyelectrolytes Tethered to Surfaces: Effect of Geometry, Acid-Base Equilibrium and Electrical Permittivity. *J. Polym. Sci., Part B: Polym. Phys.* **2006**, *44*, 2638–2662.
42. Hehmeyer, O. J.; Arya, G.; Panagiotopoulos, A. Z.; Szleifer, I. Monte Carlo Simulation and Molecular Theory of Tethered Polyelectrolytes. *J. Chem. Phys.* **2007**, *126*, 244902.
43. Solis, F. J.; de la Cruz, M. O. Collapse of Flexible Polyelectrolytes in Multivalent Salt Solutions. *J. Chem. Phys.* **2000**, *112*, 2030–2035.
44. Solis, F. J.; de la Cruz, M. O. Flexible Linear Polyelectrolytes in Multivalent Salt Solutions: Solubility Conditions. *Eur. Phys. J. E: Soft Matter Biol. Phys.* **2001**, *4*, 143–152.
45. Nap, R.; Tagliazucchi, M.; Szleifer, I. Born Energy, Acid-Base Equilibrium, Structure and Interactions of End-Grafted Weak Polyelectrolyte Layers. *J. Chem. Phys.* **2014**, *140*, 024910.
46. Jha, P. K.; Zwanikken, J. W.; de la Cruz, M. O. Understanding Swollen-Collapsed and Re-Entrant Transitions in Polyelectrolyte Nanogels by a Modified Donnan Theory. *Soft Matter* **2012**, *8*, 9519–9522.
47. Szleifer, I.; Carignano, M. A. Tethered Polymer Layers. *Adv. Chem. Phys.* **1996**, *96*, 165–260.
48. Gong, P.; Wu, T.; Genzer, J.; Szleifer, I. Behavior of Surface-Anchored Poly(Acrylic Acid) Brushes with Grafting Density Gradients on Solid Substrates: 2. Theory. *Macromolecules* **2007**, *40*, 8765–8773.